Supporting Information

Bio-inspired, Ultra-tough, High-Sensitivity, and Anti-swelling Conductive Hydrogel Strain Sensor for Motion Detection and Information Transmission

Xiang Di[a], Jiawen Hou[a], Mingming Yang[a], Guolin Wu[a,*], Pingchuan Sun[a,*]

[a]Key Laboratory of Functional Polymer Materials, Institute of Polymer Chemistry
College of Chemistry, Nankai University, Tianjin 300071, P. R. China.
E-mail: guolinwu@nankai.edu.cn spclbh@nankai.edu.cn

Experimental Section/Methods

Materials

Adenine (A) was obtained from Aladdin Reagent Company. (Shanghai. China). Acrylic acid (AA), acrylamide (AM), and potassium persulfate (KPS) were obtained from TCI. (Shanghai. China). Butanediol diacrylate, sodium chloride (NaCl, 99.5%), and 2,6-ditertbutyl-4-methylphenol were obtained from Energy Chemical. Sodium dodecyl sulfate (SDS) was supplied by Sigma-Aldrich Trading Co., Ltd. (China). Ferric chloride hexahydrate ($FeCl_3 \cdot 6H_2O$) was purchased from Heowns Biotechnology Co., Ltd. Other reagents were supplied by J&K Chemical Co., Ltd. (Beijing, China).

Synthesis of 4-((3-(adenin-9-yl)propanoyl)oxy)butyl acrylate (BA-A)

The monomer BA-A was prepared according to the method reported in the literature.[1] Briefly, adenine (8.00 g), K_2CO_3 (0.32 g), and 2,6-ditertbutyl-4-methylphenol (0.48 g) were added to dimethyl sulfoxide (160 mL), and the contents were heated at 50 °C until the solid dissolved completely. Butanediol diacrylate (24 mL) was rapidly added dropwise to the flask under vigorous stirring conditions. Finally, the entire mixed solution was poured into an excess of distilled water, washed with n-hexane, and extracted with dichloromethane. The resulting solution was dried with $MgSO_4$. The white product was then obtained in 78% yield. The structure of BA-A is illustrated in **Fig. S1**.

Fabrication of physically cross-linked conductive hydrogels

Physical ionic conductive hydrogels were fabricated by a three-step procedure via free-radical polymerization method. First, a uniform aqueous suspension of NaCl, SDS, and BA-A was prepared at room temperature. Monomers AM, AA, and KPS were then quickly added to the solution. The mixed solution was degassed under nitrogen for 30 min, poured rapidly into glass molds, and maintained at 65 °C for 12 h to yield the pristine hydrogel (P-hydrogel). Second, the P-hydrogel was immersed in aqueous solution of $FeCl_3 \cdot 6H_2O$ for 24 h to obtain a coordination hydrogel (C-hydrogel). Finally, the formed C-hydrogel was immersed in excess distilled water for 48 h to remove superfluous Fe^{3+} and obtain the equilibrium swollen hydrogel (E-hydrogel). Compositions of all the samples with different monomers are listed in **Table S1**.

Characterization

^1H NMR spectra of monomer BA-A were recorded by NMR (400 MHz, Bruker AVANCE III NMR) spectroscopy. Fourier-transform infrared (FTIR) spectroscopy (A225/Q Platinum ATR) was used to characterize the structures of BA-A and hydrogels. The morphology of lyophilized samples was systematically explored by scanning electron microscopy (SEM, Zeiss Merlin Compact, Germany).

Dynamic rheological measurement of hydrogels

Dynamic shear rheology test was performed using a rheometer (DHR-2, TA Instruments), with parallel plates (20 mm diameter). The strain sweep was conducted with a fixed frequency of 1 Hz. The frequency sweep was tested at a constant strain of 0.5%, thus avoiding a non-linear response. The microscopic self-recovery was analyzed by the alternate step strain test (0.5% and 50%) of oscillatory force at 1 Hz to characterize the rupture and rearrangement of the hydrogel network.

Mechanical measurements

The standard tensile test was conducted using a tensile instrument (UTM6103, Suns Technology Stock Co., Ltd., China). Hydrogels with thickness of 1.0 mm were cut into rectangular blocks (50 mm × 4 mm) for testing at room temperature. The stretching rate was maintained at 50 mm min^{-1} for tensile measurement and 100 mm min^{-1} for the load–unload test.

Characterization of thermodynamic properties

Differential scanning calorimetry (DSC) was used to characterize the phase transition temperature of hydrogels. The test temperature ranged from 25 to −60 °C under a nitrogen atmosphere with a cooling rate of 10 °C min^{-1} and a heating rate of 10 °C min^{-1}. Hydrogel (~10 mg) was loaded in a 40-μL aluminum pan for DSC testing.

Weight swelling ratio measurements

The weight swelling ratio is defined as the ratio of the increased mass ($M_d - M_i$) in the sample after dissolution to the initial weight of the hydrogel (M_i).

$$Weight\ swelling\ ratio(\%) = \left(\frac{M_d - M_i}{M_i}\right) * 100\% \quad (1)$$

where M_d and M_i are the mass of the hydrogel after dissolution and at initial state, respectively.

Conductivity measurements

The relative resistance of the hydrogel sensor in different states was recorded using a digital source meter (Model 2450, Keithley). The value of $\Delta R/R_0$ was calculated by using the following equation:

$$\frac{\Delta R}{R_0}(\%) = \left(\frac{R - R_0}{R_0}\right) * 100\% \quad (2)$$

where R_0 and R are the resistances of the original hydrogel sensor and the same sample that is stretched, respectively.

The GF of the sensor was calculated as follows:

$$GF = \frac{\Delta R/R_0}{\varepsilon} \quad (3)$$

where $\Delta R/R_0$ is the relative resistance change of the strain sensor and ε denotes corresponding strain change of the sample.

Low-field ^{1}H NMR spectroscopy

Low-field NMR spectroscopy was conducted using a low-field spectrometer (Bruker Minispec MQ20) with a proton resonance frequency of 20 MHz. The typical p/2 pulse length of the Minispec was ~3 μs and the dead time of the receiver was ~13 μs. Magic-sandwich echo (MSE) pulse sequence was applied to reunite the lost signal. In multiphase materials, rigid components with a strong proton dipole coupling possess fast proton signal decay, while the mobile component exhibits a slow free-induction decay (FID) signal due to the averaging effect. Therefore, the regained MSE-FID signal can be fitted to the following equation:

$$I(t) = f_r exp\left(-\left(t/T_{2r}\right)^2\right) + f_i exp\left(-\left(t/T_{2i}\right)^{n_i}\right) + f_s exp\left(-\left(t/T_{2s}\right)^{n_s}\right) \quad (4)$$

where f_r, f_i, and f_s represent the relative contents of the rigid component, intermediate component, and soft component, respectively, and $f_r+f_i+f_s = 1$. T_{2r}, T_{2i}, and T_{2s} indicate the relaxation time of the rigid component, intermediate component, and mobile component, respectively ($T_{2r} < T_{2i} < T_{2s}$).

Proton MQ NMR experiments

NMR spectroscopy is a convenient and accurate technique to obtain information about the dynamics of polymer networks and solid structures. In general, two sets of data, the double quantum (DQ) and the reference signal intensity (I_{DQ} and I_{ref}), can be obtained from MQ NMR experiments. The sum of these two signals is the MQ intensity, which is affected by chain segment fluctuations. Therefore, it needs to be normalized in order to obtain the normalized DQ intensity as follows:

$$I_{nDQ}(\tau_{DQ}) = \frac{I_{DQ}(\tau_{DQ})}{I_{\sum MQ}(\tau_{DQ})} \quad (5)$$

Such a normalization process eliminates the temperature-dependent chain segment kinetic effects so that the normalized DQ intensity accumulation is completely dependent on the network and the D_{res} is determined by the confined structure.

Table S1. Compositions of hydrogels

Hydrogels	AM (mmol)	BA-A (molar ratio of AM)%	AA (molar ratio of AM)%	Fe^{3+} (mol L^{-1})	KPS (mg)	Water (mL)
E-BA-A-0.0	70	0.0	15	0.06	40	10
E-BA-A-0.25	70	0.25	15	0.06	40	10
E-BA-A-0.5	70	0.5	15	0.06	40	10
E-BA-A-1.0	70	1.0	15	0.06	40	10
E-BA-A-2.0	70	2.0	15	0.06	40	10
E-AA -10	70	0.5	10	0.06	40	10
E-AA-20	70	0.5	20	0.06	40	10
E-AA-25	70	0.5	25	0.06	40	10
E-Fe-0.01	70	0.5	15	0.01	40	10
E-Fe-0.03	70	0.5	15	0.03	40	10
E-Fe-0.12	70	0.5	15	0.12	40	10

Table S2. Summary of recently reported high-strength iron ion coordination hydrogels

Sample	Toughness (MJ m^{-3})	Strain (%)	Stress (MPa)	Source
P(AM-BA-A-AA)/Fe^{3+}	58.415	2044	4.454	This study
P(AM-SMA-AA)/Fe^{3+}	53	1025	6.8	Ref.1[2]
P(AAm-co-AAc)/Fe^{3+}	1.3	200	7.1	Ref.2[3]
PAA-CNF-Fe^{3+}	11.05	1803	1.37	Ref.3[4]
P(AM-UPy-AA)/Fe^{3+}	28.06	642	6.3	Ref.4[5]
HP(AAm/AA)-CS-Fe^{3+}	23.8	1300	2.75	Ref.5[6]
PAAm/PAA-Fe^{3+}/NaCl	3.64	475	1.2	Ref.6[7]
P(AM-co-AA)/Na-Alginate/Fe^{3+}	4.8	225	10.4	Ref.7[8]
P(AM-co-AA)/clay/Fe^{3+}	49.11	2113	3.52	Ref.8[9]
PAA/CS/GO/Gly/Fe^{3+}	1.124	1100	0.226	Ref.9[10]
P(AM-co-AA)/Fe^{3+}	27.5	748	5.9	Ref.10[11]

Table S3. Summary of recently reported comprehensive properties of conductive hydrogels

Sample	Response time (ms)	Strain (%)	Stress (MPa)	Mimi-detection strain (%)	Toughness (MJ m^{-3})	Source
P(AM-BA-A-AA)/Fe^{3+}	47.7	2044	4.454	0.2	58.415	This study
PAA/CS/GO/Gly	97	1100	0.226	0.25	1.124	Ref.1[10]
A_6PC_{23}	155	1250	0.5	5	2.5	Ref.2[12]
MXene/PVA	165	1200	-	20	-	Ref.3[13]
Agar/NaCl/PAM DN	100	1920	0.4	0.5	4	Ref.4[14]
HPAAm/CS-c-MWCNT	151	2761	0.065	-	0.8	Ref.5[15]
$MG_{40}P_{0.03}$	200	2850	0.298	1	-	Ref.6[16]
HP(AAm/AA)-CS-Fe^{3+}	-	1300	2.75	10	23.8	Ref.7[6]
P(AM-BA-A-ACG)	97.23	681	0.217	2.5	0.64	Ref.8[17]
PAAm-oxCNTs	300	1041	0.71	50	2.29	Ref.9[18]
PAAm/CMC	360	371	0.0146	-	-	Ref.10[19]
PAC hydrogel	800	1700	0.385	20	-	Ref.11[20]
PVA-CNF-o-gel	-	660	2.1	25	5.25	Ref.12[21]

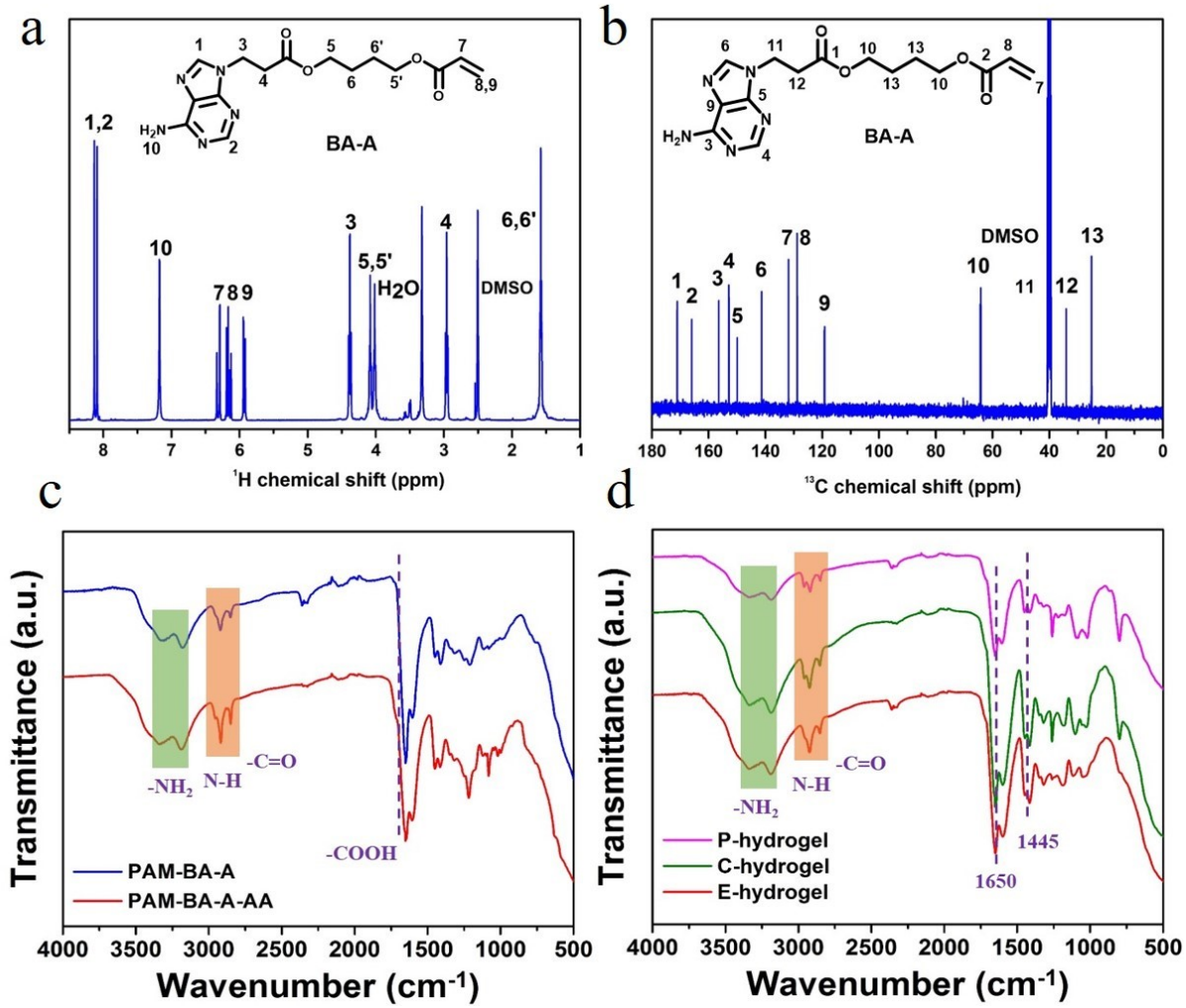

Fig. S1 (a) ^{1}H NMR and ^{13}C NMR spectra of BA-A in DMSO-d_6, (c) FTIR spectra of PAM-BA-A and PAM-BA-A-AA polymers, and (d) FTIR spectra of P.C.E-hydrogel.

^{1}H NMR spectrum of BA-A (DMSO-d_6, 400 MHz): d 8.13–8.09 (d, 2H, H_{1+2}), 7.15 (s, 2H, H_{10}), 6.33–5.91 (m, 3H, H_{7+8+9}), 4.38 (m, 2H, H_3), 2.96 (m, 2H, H_4), 4.08–4.02 (m, 4H, $H_{5+5'}$), 1.57–1.59 (m, 4H, $H_{6+6'}$) ppm. ^{13}C NMR spectrum of BA-A (DMSO-d_6, 100 MHz, δ ppm): 171.1, 165.9, 156.4, 152.6, 141.2, 131.9, 128.8, 119.1, 64.1, 33.9, 25.2.

In the spectrum of PAM-BA-A-AA, the peaks appearing at 1646 and 1708 cm^{-1} are attributed to the C=O stretching vibrations of the amide and carboxyl groups, respectively, while the signals of N–H bending and stretching appear at 1546 and 3315 cm^{-1}, respectively. Noteworthy, the absorption peak at 1708 cm^{-1} corresponds to the characteristic peak of –COO– of AA. This peak appears for the PAM-BA-A-AA polymer, but not for the PAM-BA-

A polymer, indicating the successful preparation of the PAM-BA-A-AA polymer. Characteristic bands at 1700–1600 cm^{-1} and 1500–1400 cm^{-1} are attributed to –COO– stretching vibrations. The results indicate the formation of copolymers of AM and AA. The changes in the characteristic peaks at 1700–1600 cm^{-1} and 1500–1400 cm^{-1} indicate the formation of ionic coordination bonds between Fe^{3+} and carboxyl groups.

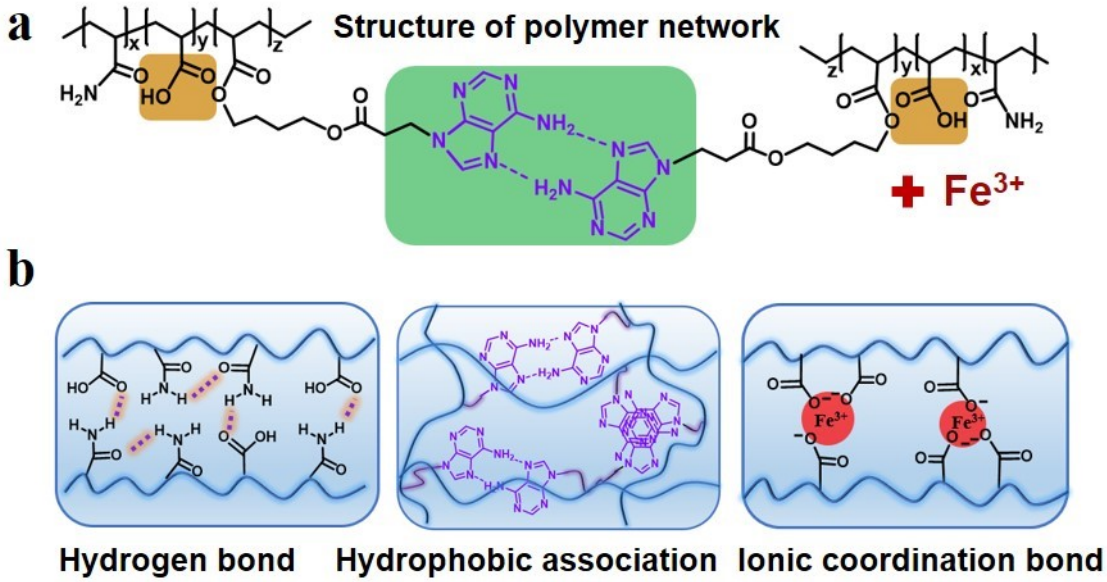

Fig. S2 (a) The polymer structure of E-hydrogel, (b) Multiple physical interactions in E-hydrogels, including inter/intra-molecular hydrogen bonding, π–π stacking of hydrophobic–conjugated microregion structural domains, and ionic coordination bond.

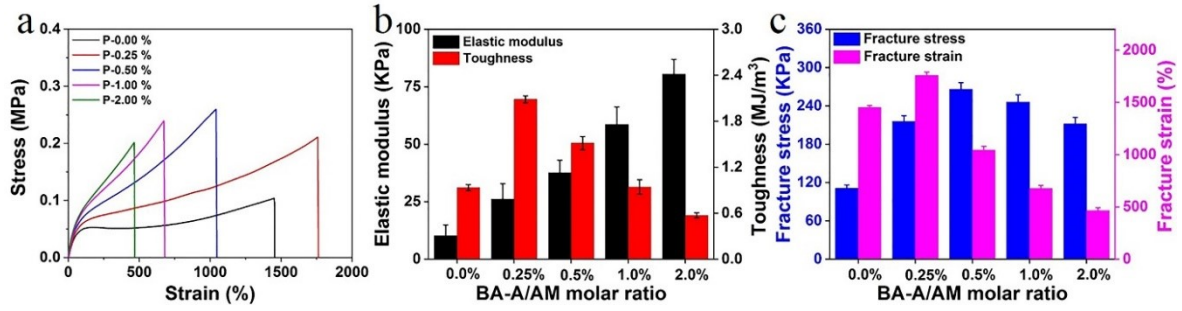

Fig. S3 (a) Tensile curves and the corresponding (b) elastic modulus, toughness, (c) fracture stress, and strain of P-hydrogel crosslinked with BA-A/AM with different contents.

The effect of BA-A content on mechanical properties of P-hydrogel was studied. **Figs. S3a–c** demonstrate that the elastic modulus of P-hydrogels increased with the increase in the

content of BA-A. The fracture stress, fracture strain, and toughness of P-hydrogel improved with the addition of BA-A. However, with the increase in the molar ratio from 0.25% to 2%, the fracture strain and toughness of P-hydrogel declined gradually, which could be ascribed to hydrophobic association with a strong and stable physical interaction. With the increase of BA-A content, more crosslinking domains of hydrophobic interaction were formed and the corresponding strength of hydrophobic association was also reinforced consequently, resulting in the enhancement of the rigidity of polymer network. However, continuous increase of the aggregation of hydrophobic blocks reduced the flexibility of the polymer chain, leading to the degeneration of the elongation at break and toughness.

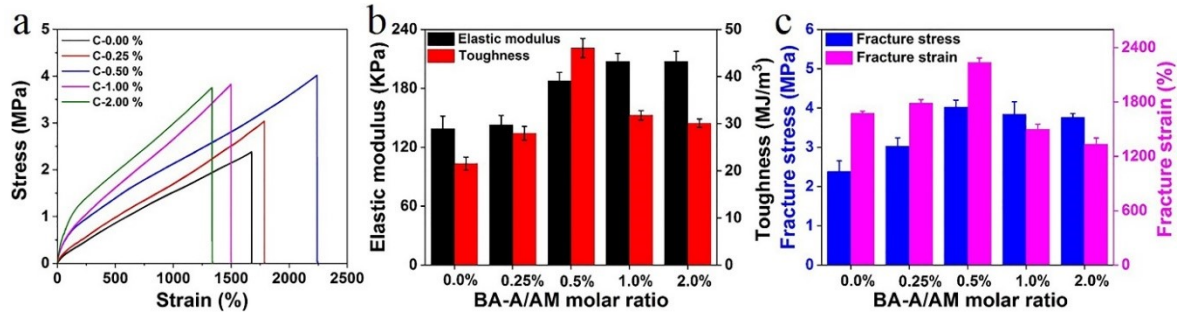

Fig. S4 (a) Tensile curves and the corresponding (b) elastic modulus, toughness, (c) fracture stress and strain of C-hydrogel crosslinked with BA-A/AM with different contents.

Fig. S4 shows the effect of BA-A content on mechanical properties of C-hydrogel. The P-hydrogel was immersed in aqueous solution of Fe^{3+} (0.06 M) for 24 h to form C-hydrogel. Obviously, the introduction of ionic coordinate interactions could significantly improve the mechanical strength, elastic modulus, and toughness. The corresponding parameter trend was similar to that of P-hydrogel; however, when BA-A content was 0.5%, the hydrogel exhibited the optimal mechanical properties, which was due to the synergistic interaction between strong coordination of Fe^{3+} and hydrophobic association.

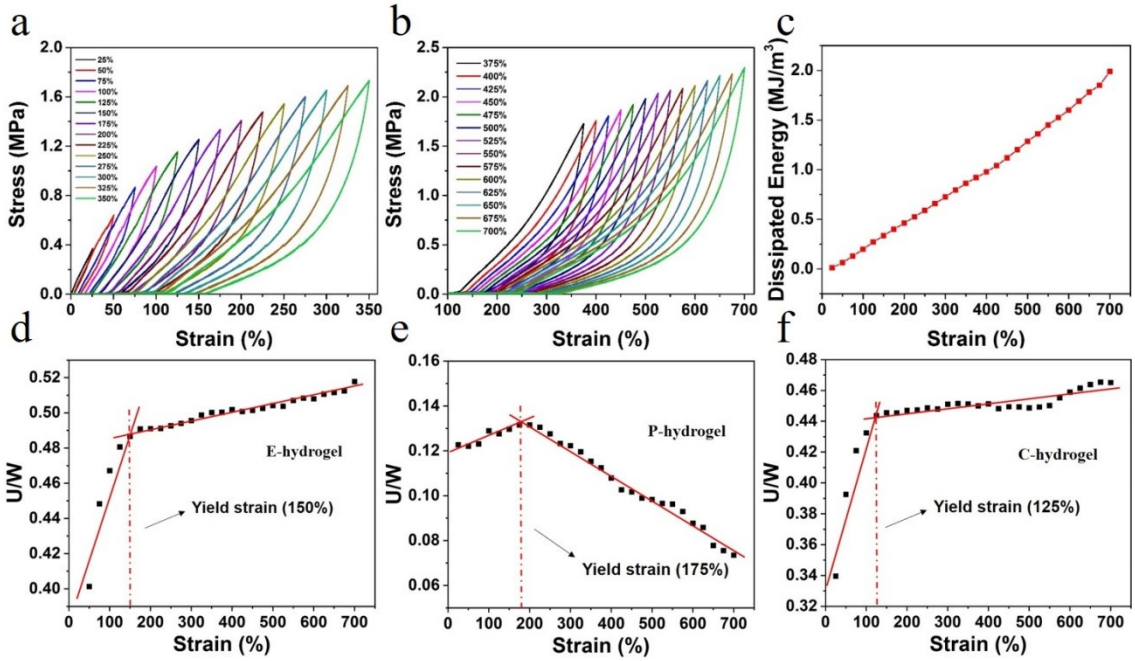

Fig. S5 Hysteresis loops of E-hydrogels measured in cyclic tensile test at (a) small and (b) large strains, (c) Dissipated energy (U), and (d) ratio of dissipated energy and work of extension, U/W, as a function of strain, (e) The ratio of dissipated energy and work of extension, U/W, as a function of strain of P-hydrogel, and (f) C-hydrogel.

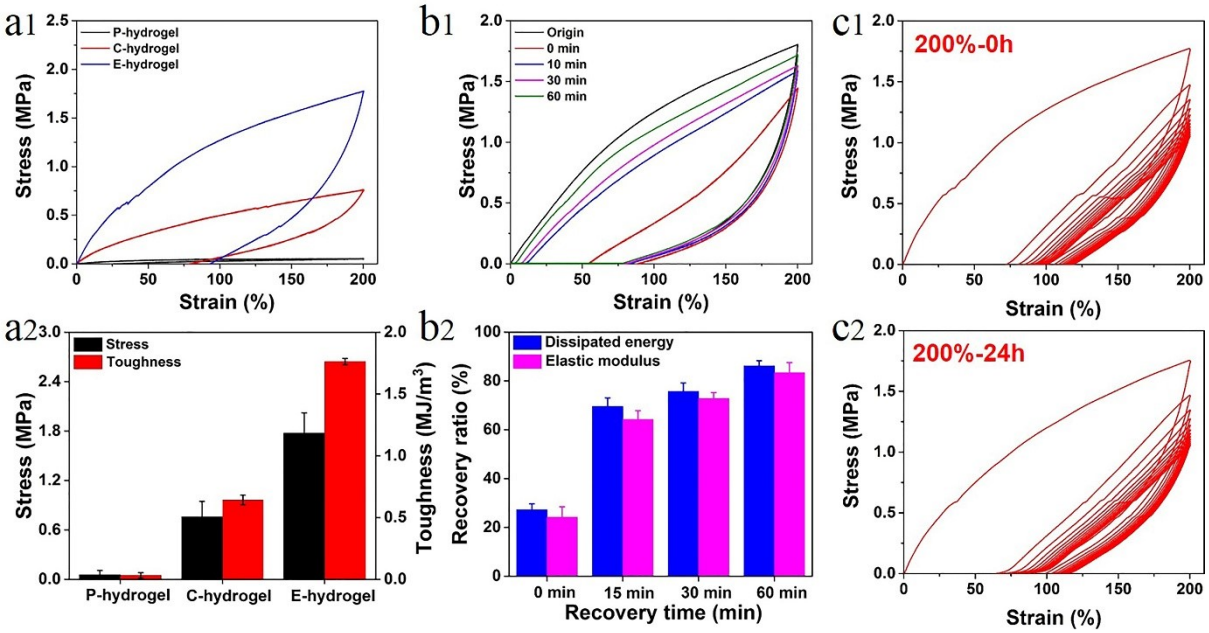

Fig. S6 (a1) Load–unload curves of P.C.E-hydrogel with a strain of 200% and (a2) the corresponding stress and toughness; (b1) Cyclic loading curves of E-hydrogel under a strain of 200% and (b2) the time-dependent recovery of elastic modulus and dissipated energy; and

(c1) Ten successive load–unload cycles of E-hydrogel and (c2) restored hydrogel after 24 h resting time.

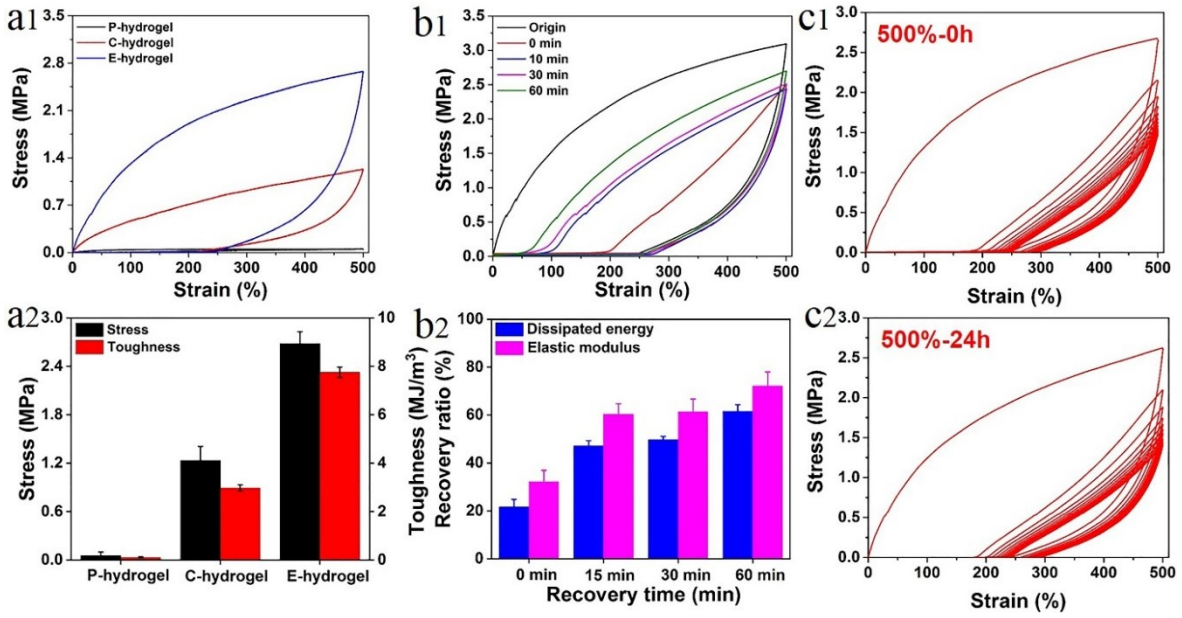

Fig. S7 (a1) Load–unload curves of different hydrogel with a strain of 500% and (a2) corresponding stress and toughness; (b1) Cyclic loading curves of E-hydrogel under a strain of 500% and (b2) the time-dependent recovery of elastic modulus and dissipated energy; and (c1) Ten successive load–unload cycles of E-hydrogel and (c2) the restored hydrogel after 24 h resting time.

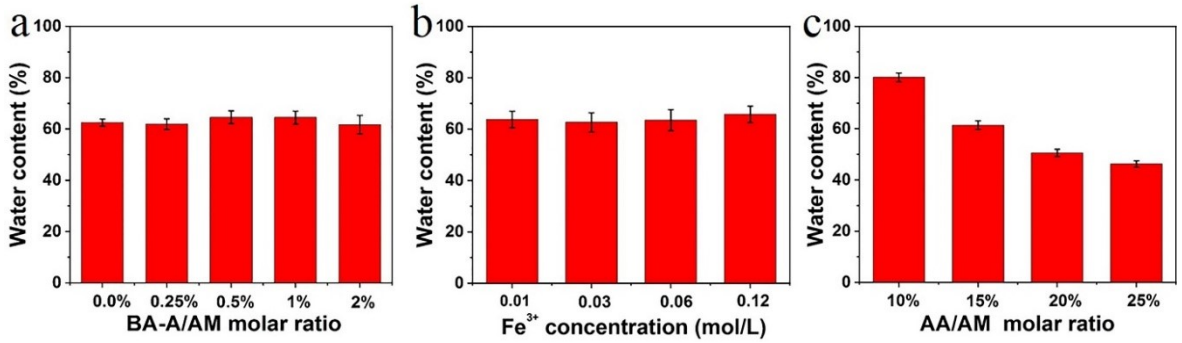

Fig. S8 Water content of E-hydrogel at different BA-A/AM, Fe^{3+}, and AA/AM concentrations.

The water content of hydrogels with different compositions was investigated, as shown in **Fig. S8. Figs. S8a, b** exhibit little difference in water content, indicating that the coordination between carboxylic acid and iron ion had reached equilibrium. **Fig. S8c** shows that with the increase of AA content, the water content of hydrogel decreased from 80±1.67%

to 50.5±1.4%, which was attributed to the fact that the excessive content of the AA monomer could lead to the increase of crosslinking density of the E-hydrogels[5, 9, 11] that became too high and formed inner sparse layers and outer dense structures of the monomer bit by bit, resulting in observed reduction in the water content of hydrogels.

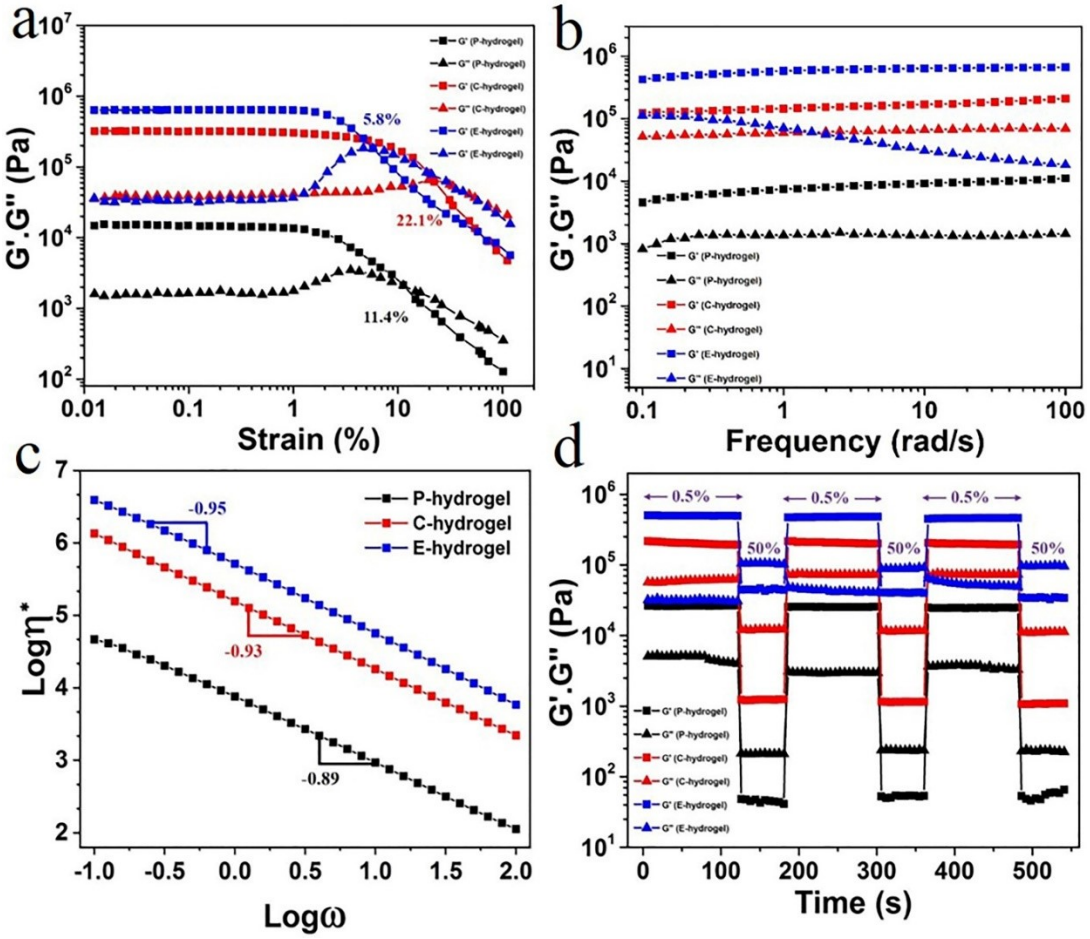

Fig. S9 (a) Rheology behavior under shear strain and (b) angular frequency; (c) Complex viscosity (η*) as a function of oscillatory frequency (ω); (d) G′ and G″ of hydrogel at alternate strain between subtle (0.5%) and large strain (50%) with fixed frequency (1 Hz).

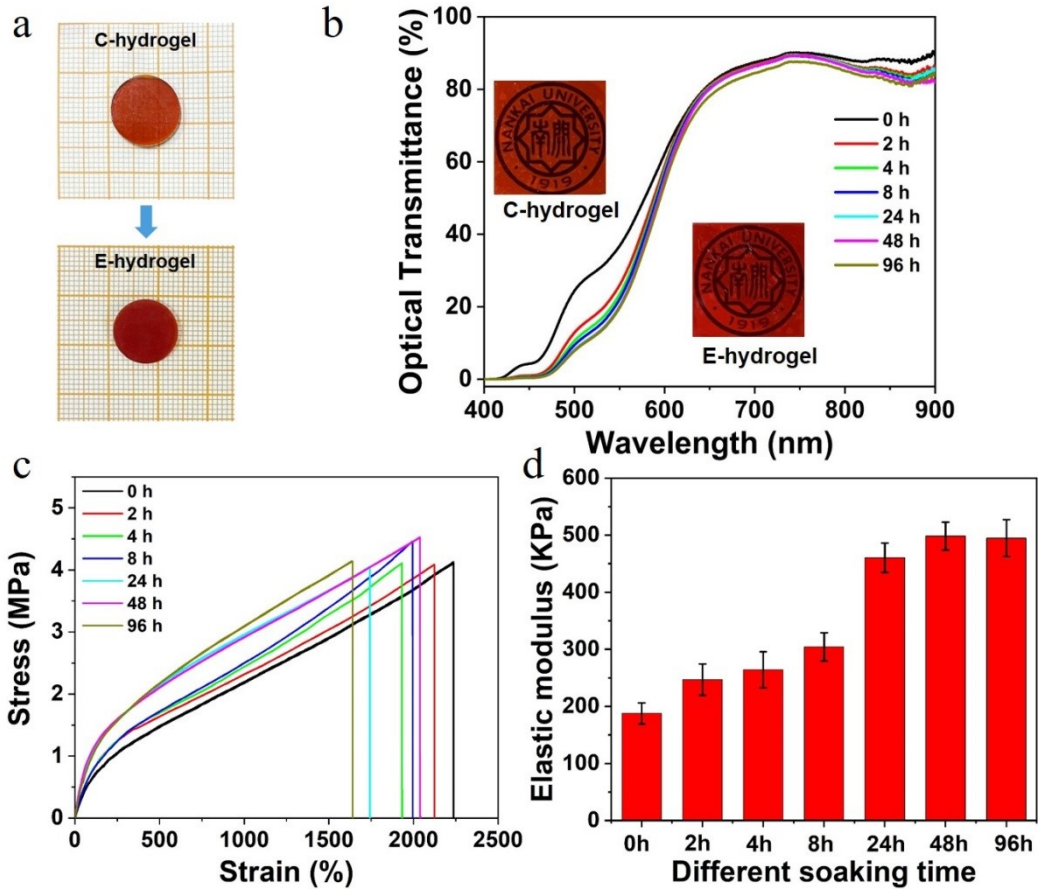

Fig. S10 (a) The color and volume changes of different hydrogels; (b) Optical transmittance of hydrogels in the wavelength range of 400 to 900 nm for different soaking times; (c, d) Tensile stress–strain curves and the corresponding elastic modulus of hydrogels for different soaking time.

Fig. S10a exhibits the color and volume changes of C.E-hydrogel. The results indicate that when E-hydrogel is immersed in deionized water, its volume shrinks and the color changes from red to deep red. Moreover, deionized water turns to slight yellow color. The evidence further indicates that superfluous Fe^{3+} diffused into hydrogel, as a result, a mixture of mono-, bi-, and tri-dentates was formed. When immersed in water, excess Fe^{3+} diffused out of hydrogel and reorganization of coordinates occurred to form more tridentate structure inside hydrogel. **Fig. S10b** illustrates that the transmittance of E-hydrogel also decreased over the entire wavelength range with increasing soaking times from 0 to 24 h. However, the transmittance remained essentially stable after the hydrogel was immersed in deionized water

for 48 h. Furthermore, tensile stress–strain curves and the corresponding elastic modulus of hydrogels for different soaking time are shown in **Figs. S10c, d**. Clearly, the hydrogel exhibited a stable elastic modulus after immersion for 48 h; and therefore, the above-mentioned results indicate that reorganization of coordinates occurred to form more tridentate structure and reached a saturated state after immersion in water.

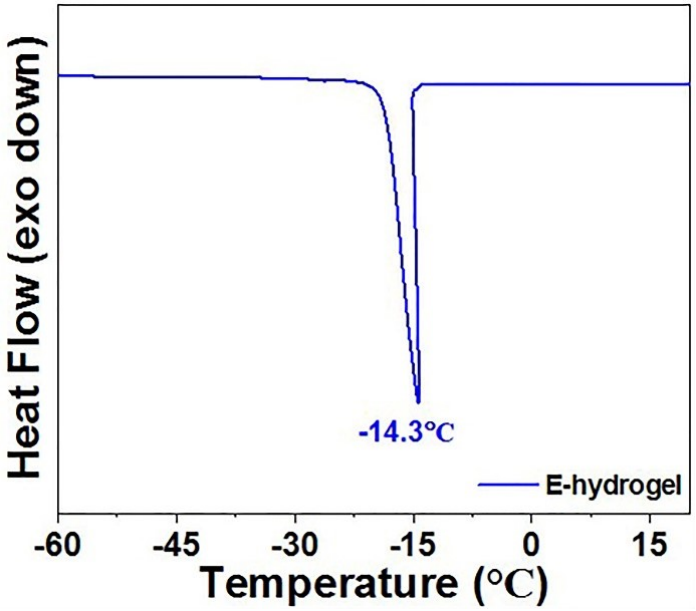

Fig. S11 DSC curves of E-hydrogel.

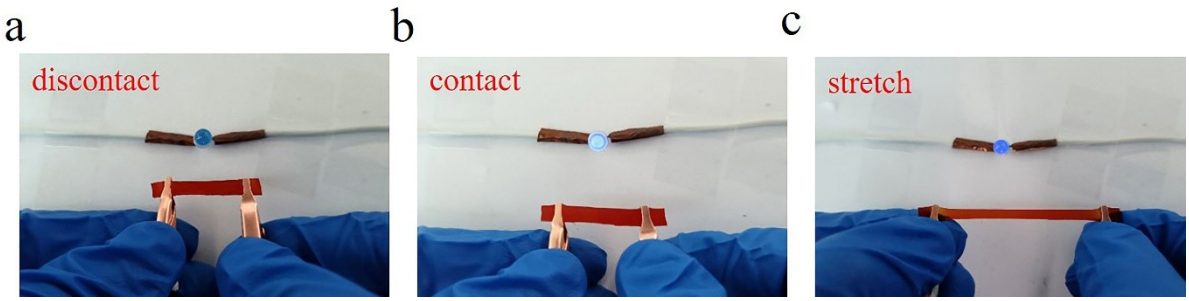

Fig. S12 Photographs of changes in LED brightness under (a) discontact, (b) contact, and (c) stretch state.

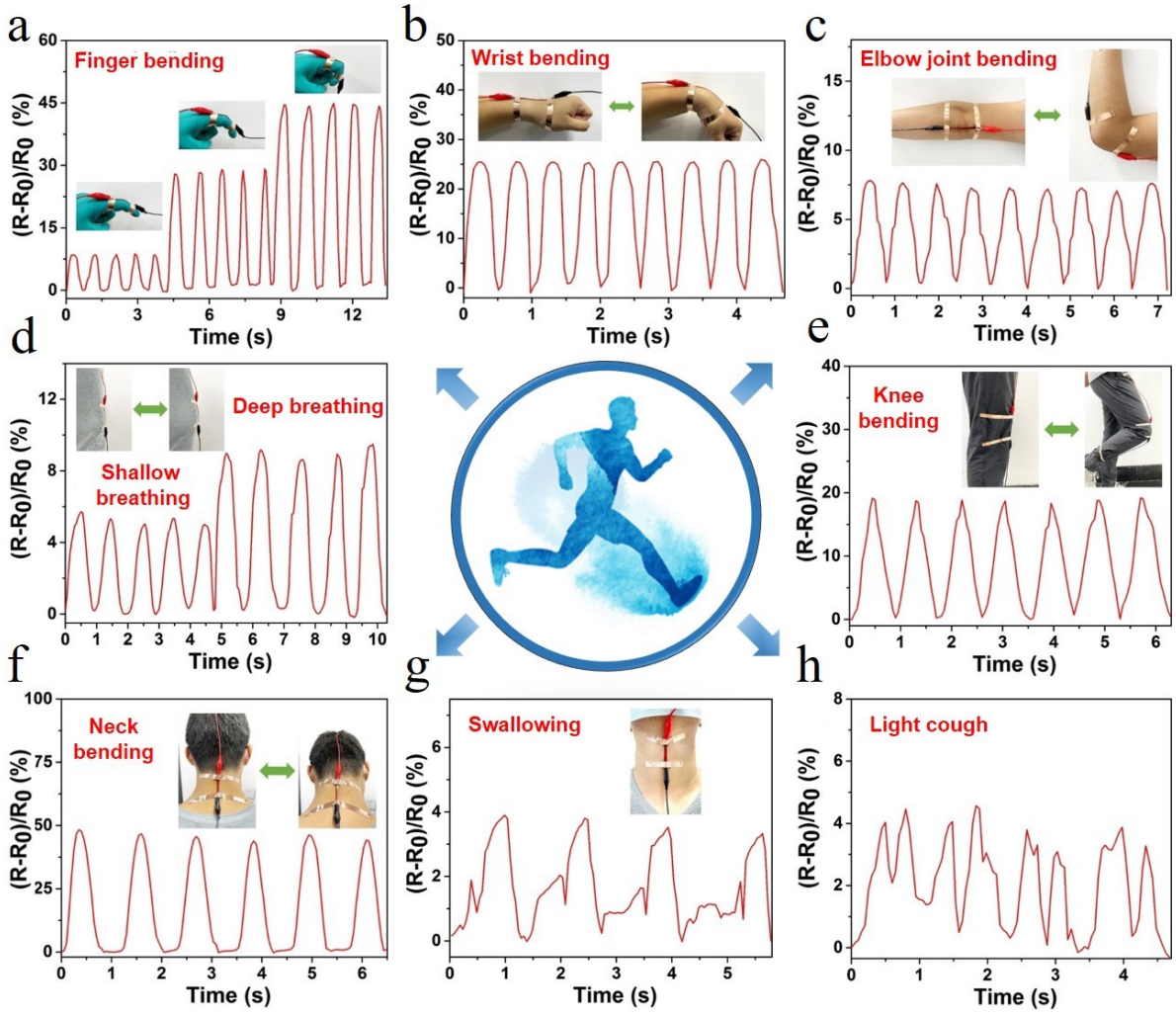

Fig. S13 Detection of different movements of human body in real time as the sensor was fixed on the (a) finger, (b) wrist, (c) elbow, (d) breathing system, (e) knee joint, and (f) neck. Subtle muscle movements of the throat with (g) swallowing and (h) light cough.

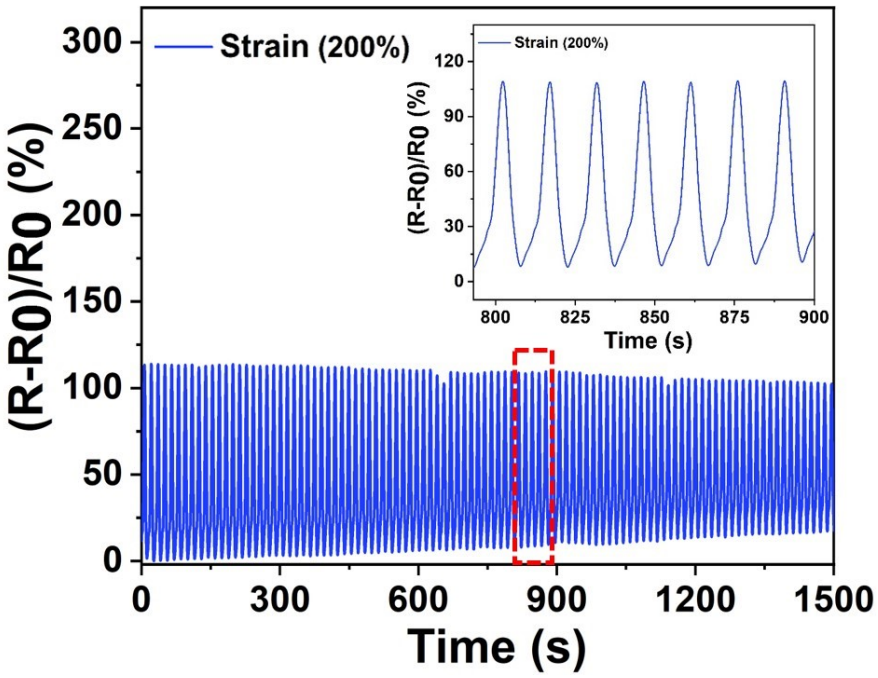

Fig. S14 Stability of relative resistance signals of the sensor at the strain of 200% for 100 cycles.

In order to further assess the stability and durability of the sensor, it was subjected to 100 consecutive tensile cycles at 200% strain. Importantly, no obvious loss of electric signal was observed during the process of consecutive stretching and releasing processes, indicating the excellent stability and repeatability of the hydrogel-based sensors.

References

1. S. Cheng, M. Zhang, N. Dixit, R. B. Moore and T. E. Long, *Macromolecules*, 2012, **45**, 805-812.
2. Z. Qin, R. Niu, C. Tang, J. Xia, F. Ji, D. Dong, H. Zhang, S. Zhang, J. Li and F. Yao, *Macromol. Mater. Eng.*, 2018, **303**, 1700396.
3. S. Y. Zheng, H. Ding, J. Qian, J. Yin, Z. L. Wu, Y. Song and Q. Zheng, *Macromolecules*, 2016, **49**, 9637-9646.
4. C. Shao, H. Chang, M. Wang, F. Xu and J. Yang, *ACS Appl. Mater. Interfaces,* 2017, **9**, 28305-28318.
5. T. Liu, S. Zou, C. Hang, J. Li, X. Di, X. Li, Q. Wu, F. Wang and P. Sun, *Polym. Chem*, 2020, **11**, 1906-1918.
6. J. Xu, R. Jin, X. Ren and G. Gao, *J. Mater. Chem. A*, 2019, **7**, 25411-25448.
7. S. Li, H. Pan, Y. Wang and J. Sun, *J. Mater. Chem. A*, 2020, **8**, 3667-3675.
8. Y. Liang, J. Xue, B. Du and J. Nie, *ACS Appl. Mater. Interfaces*, 2019, **11**, 5441-5454.
9. Y. Hu, Z. Du, X. Deng, T. Wang, Z. Yang, W. Zhou and C. Wang, *Macromolecules*, 2016, **49**, 5660-5668.
10. S. Xia, S. Song, Y. Li and G. Gao, *J. Mater. Chem. C*, 2019, **7**, 11303-11314.
11. P. Lin, S. Ma, X. Wang and F. Zhou, *Adv. Mater.*, 2015, **27**, 2054-2059.
12. R. Liu, H. Wang, W. Lu, L. Cui, S. Wang, Y. Wang, Q. Chen, Y. Guan and Y. Zhang, *Chem. Eng. J.*, 2021, **415**, 128839.
13. J. Zhang, L. Wan, Y. Gao, X. Fang, T. Lu, L. Pan and F. Xuan, *Adv. Electron. Mater.*, 2019, **5**, 1900285.
14. W. Hou, N. Sheng, X. Zhang, Z. Luan, P. Qi, M. Lin, Y. Tan, Y. Xia, Y. Li and K. Sui, *Carbohydr. Polym.*, 2019, **211**, 322-328.
15. S. Xia, S. Song, F. Jia and G. Gao, *J. Mater. Chem. B*, 2019, **7**, 4638-4648.
16. H. Sun, Y. Zhao, C. Wang, K. Zhou, C. Yan, G. Zheng, J. Huang, K. Dai, C. Liu and C. Shen, *Nano Energy*, 2020, **76**, 105035.
17. X. Di, J. Li, M. Yang, Q. Zhao, G. Wu and P. Sun, *J. Mater. Chem. A*, 2021, **9**, 20703–20713.
18. X. Sun, Z. Qin, L. Ye, H. Zhang, Q. Yu, X. Wu, J. Li and F. Yao, *Chem. Eng. J.*, 2020, **382**, 122832.
19. T. Zhu, Y. Cheng, C. Cao, J. Mao, L. Li, J. Huang, S. Gao, X. Dong, Z. Chen and Y. Lai, *Chem. Eng. J.*, 2020, **385**, 123912.
20. H. Sun, K. Zhou, Y. Yu, X. Yue, K. Dai, G. Zheng, C. Liu and C. Shen, *Macromol. Mater. Eng.*, 2019, **304**, 1900227.
21. Y. Ye, Y. Zhang, Y. Chen, X. Han and F. Jiang, *Adv. Funct. Mater.*, 2020, 2003430.